### 2.6 Geometrical acceptance

While HERA may produce elastic $J/\psi$ in the range $m_{J/\psi} + m_p(4\text{GeV}) < \sqrt{s_{\gamma p}} < \sqrt{s}(296\text{GeV})$, the accessible range of $\sqrt{s_{\gamma p}}$ for ZEUS detector is limited by its geometrical acceptance.

The ZEUS detector, a nearly hermetric detector, covers 99.7% of the $4\pi$ solid angle, leaving only the beam pipes uninstrumented. However, only for $J/\psi$ produced at rest in the detector and decayed isotropically, is the geometrical acceptance 99.7%. A $J/\psi$ moving at relativistic speed toward the forward(rear) beampipe perceives an inflation of the forward(rear) beampipe. The geometrical acceptance reduces to zero if either beampipe inflates to $2\pi$. The ZEUS central tracking chamber covers an even smaller solid angle. For the discussion of this chapter, we take $20°$-$160°$ as the well covered area(94% of the $4\pi$ solid angle). This section discusses how the accessible kinematical phase space is limited by the incomplete geometrical coverage.

A kinematic configuration of the $l^+l^-$ pair in the detector corresponds to a point $(s_{\gamma p}, t, \cos\theta_{1'}, \phi_{1'})$ in the phase space. The boundary of the tracking coverage maps to a surface in this phase space, where $(\cos\theta_{1'}, \phi_{1'})$, the anglular coordinates of $l^+$ as seen in $J/\psi$ rest frame, relate to $(\cos\theta_1, \phi_1)$ as measured in the detector by a Lorentz transformation with a boost determined by $(s_{\gamma p}, t)$. If the $J/\psi$ boost is small, the effect of Lorentz transformation is small. If the $J/\psi$ boost is large, the effect of small $|t|$ of $J/\psi$ is negligible. For the purpose of this section, it is mathematically simpler and physically more illustrative to discuss how a one dimensional Lorentz boost maps the boundary of the tracking chamber to the $(s_{\gamma p}, \cos\theta_1)$ phase space($\phi_1$ is integrated out). Result of the Lorentz transformation is summarized in the following equation:

$$
\begin{aligned}
\frac{1-\beta}{1+\beta} &= \frac{1-\cos\theta_1}{1+\cos\theta_1}\frac{1+\cos\theta_1'}{1-\cos\theta_1'} \\
&= \frac{1-\cos\theta_2}{1+\cos\theta_2}\frac{1-\cos\theta_1'}{1+\cos\theta_1'}
\end{aligned}
\tag{29}
$$

where $\cos\theta_1(\cos\theta_2)$ is that of $l^+(l^-)$ measured in the laboratory frame and $\cos\theta_1'$ is that of $l^+$ measured in $J/\psi$ rest frame ($\cos\theta_2' = -\cos\theta_1'$ in that frame). $\beta$ can be determined either by $s_{\gamma p}$ or $y_{\rm rap}$(the true rapidity of $J/\psi$) from following equations.

$$\begin{aligned} \frac{s_{\gamma p} - m_p^2}{2m_{J/\psi}E_p} &= \frac{E_{J/\psi}}{m_{J/\psi}} - \frac{p_{z,J/\psi}}{m_{J/\psi}} \\ &= \sqrt{\frac{1-\beta}{1+\beta}} \end{aligned} \tag{30}$$

$$\begin{aligned} y_{\rm rap} &= \log\sqrt{\frac{E_{J/\psi}+p_z}{E_{J/\psi}-p_z}} \\ &= \log\sqrt{\frac{1+\beta}{1-\beta}} \end{aligned} \tag{31}$$

Eliminating $\beta$ from Eq. (31) and Eq. (29) and substituting $\theta_{1,2}$ with boundary values 20° and 160° result in the $\theta_{1,2}$ contours in $(\cos\theta_1', y_{\rm rap})$ plane, as shown in Figure 8. We use $y_{\rm rap}$ instead of $s_{\gamma p}$ because from dynamics the distribution in $\log s_{\gamma p}$ which is proportional to $y_{\rm rap}$(see Eq. (31)) is more uniform than in $s_{\gamma p}$. Another advantage of plotting in $y_{\rm rap}$ is that it makes clear that the accessible range in $\frac{s_{\gamma p}-m_p^2}{2m_{J/\psi}E_p}$ is independent of $m_{J/\psi}$ and $E_p$. This is understandable, since the Lorentz boost affects rapidities of all tracks by the same translation and therefore it is most natural and convenient to use rapidity to study the beamhole effects. This helps to estimate the geometrical acceptance to background of low invariant mass, geometrical acceptance at different proton beam energy and so on. It is interesting to note that the electron beam energy($E_e$) does not affect the geometrical acceptance so long as $\sqrt{s_{\gamma p}}$ covered by tracking chamber is well within $\sqrt{s}$.

Figure 8(a) shows that in $J/\psi$ rest frame, holes of detector seem expanded if $J/\psi$ moves fast along the beam axis. Figure 8(b) and Eq. (31) show the relation between $J/\psi$ rapidity and $\sqrt{s_{\gamma p}}$.

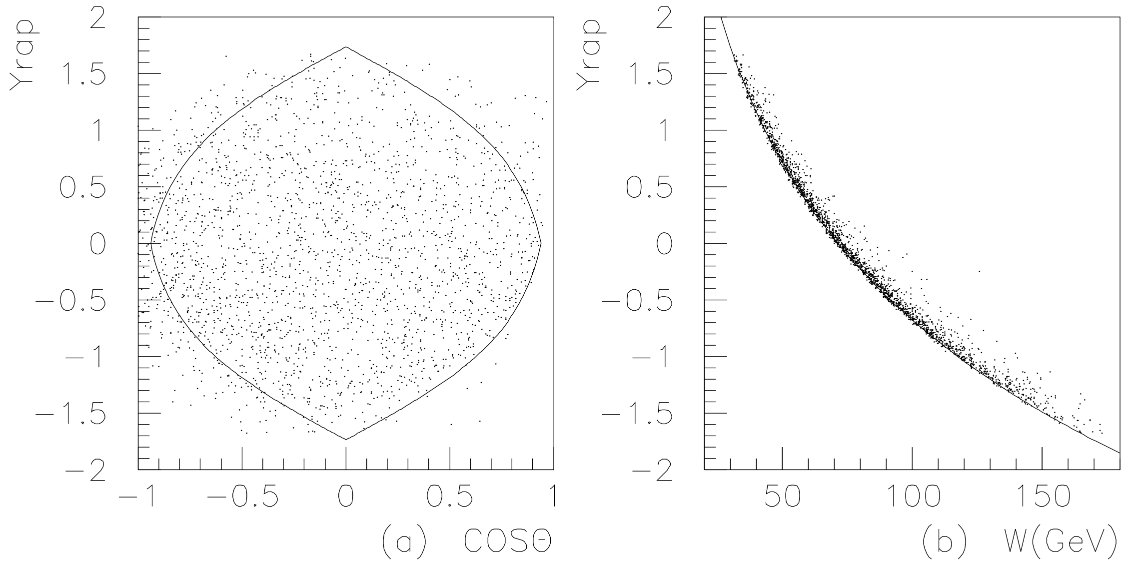


**Figure 8:** (a) The vertical axis is the true rapidity of $J/\psi$. The horizontal axis is $\cos\theta$ of $l^+$ in $J/\psi$ rest frame with respect to the proton beam axis. Area enclosed by the four curves(calculated with the assumption that $J/\psi$ momentum vector is parallel to the $ep$ beam axis) are covered by the tracking chamber, from 20° to 160° in the detector. Scattered spots are generated within 20° to 160° by a Monte Carlo $J/\psi$ event generator. As a result of nonzero transverse momentum of $J/\psi$, some events lie outside of the theoretical boundaries. (b) Scatter plot of true rapidity of $J/\psi$ vs $W$ by the same Monte Carlo generator. The solid line is the analytical relation for $p_{t,J/\psi} = 0$ case. Most of the generated events lie closely to the solid curve, reflecting $p_t$ is small in most of $J/\psi$ events. $W$-$y_{\rm rap}$ relation depends on $E_p$ and $m_{J/\psi}$.

### 2.7 Estimation on number of signal events

The number of observed events depends on several quantities.

$$N = \mathcal{L}_{ep} F_{\gamma/e} \sigma_{\gamma p} B \epsilon \tag{32}$$